Aerothermodynamic Characteristics of Slender Ablating Re-Entry Vehicles

H. G. TIMMER,* C. L. ARNE,† T. R. STOKES JR.,‡ AND H. H. TANG§
McDonnell Douglas Astronautics Company-West, Huntington Beach, Calif.

A computer program for accurately estimating the static aerodynamic characteristics of a slender, ablating re-entry vehicle is described. The approach includes a complete coupling between the flowfield analysis and the thermochemical analysis of the response of the heat shield material to the external environment. Moderate angles of attack and Mach numbers ranging from supersonic to hypersonic are considered. The transient thermochemical analysis provides values of wall temperature, mass ablation rate, and recession rate which are used to modify the vehicle shape and perform the flowfield calculations at the next trajectory point.

Nomenclature

A_{ref} = reference area
a_j = zeros of Legendre polynomials
B = blowing parameter
C_D, C_f = drag and skin-friction coefficients
C_H = Stanton number
C_l, C_m = rolling and pitching moment coefficients
C_n, C_p = normal force and pressure coefficients
c_p = specific heat
E^* = activation energy
f_B = resin fraction
h, H = enthalpy and total enthalpy, $H = h + u_e^2/2$
Δh = reference heat of formation
ℓ = exponent in the assumed velocity profile $U/Ue = (y/\delta_o)^{1/\ell}$
k = thermal conductivity
K = hypersonic similarity parameter, $K = (M_\infty^2 - 1)^{1/2}\xi$, or mass fraction
L_{ref} = reference length
M = Mach number
$\dot{m}$ = mass transfer rate
$\hat{n}$ = unit surface normal vector
n = reaction order
N_c = enthalpy-based heat transfer coefficient
ΔN = incremental surface recession distance
p = pressure
q = heat transfer rate
ΔQ = surface energy of decomposition or combustion
r = stream-tube radius
$\mathbf{r}$ = position vector of a point measured in a body-fixed coordinate system
$\mathbf{r}_{c.g.}$ = vector connecting the vehicle center of gravity with a given point on the body
R_{e_s} = Reynolds number based on running length
s = running length
$\dot{s}$ = surface recession rate
S = surface area
t = time
$\hat{t}$ = unit vector in the surface streamline direction
T = temperature
U = one-dimensional array $(u^3, u^2, u, 1)$
$u, \mathbf{u}$ = velocity along the body, or surface parameter; $\mathbf{u} = u/u_e$
w = surface parameter
W = one-dimensional array, $(w^3, w^2, w, 1)$
W_j = weighting functions associated with Legendre polynomials
y = coordinate normal to the surface
α = vehicle angle of attack
α_s = surface absorption coefficient
β, β_s = yaw angle and shock angle, respectively
γ = ratio of specific heats
γ' = char fraction
δ, δ^* = boundary-layer thickness and displacement thickness
δ^{**}, Δ^* = boundary layer momentum thickness and effective value
σ = axisymmetric parameter: $\sigma = 0$ for two-dimensional flow, $\sigma = 1$ for axisymmetric flow
ζ = transverse curvature parameter
ϕ = meridian angle measured from the windward meridian
θ_c = cone half-angle
μ = coefficient of viscosity
ξ = effective local inclination, $\xi = -\hat{U}_\infty \cdot \hat{n}$
ρ = density

Subscripts

a, c, d = air, char, and pyrolysis decomposition
e = edge of boundary layer
g = internal gaseous mass transfer
M = mechanical removal
$_0, r$ = nonblowing value and recovery value
R, RR = radiative and reradiative heat transfer
sp, T = stagnation point and total conditions
t = transition
tvc = transverse curvature
w, ∞ = wall and freestream
$*$ = Eckert reference condition

Presented as Paper 70-826 at the AIAA 5th Thermophysics Conference, Los Angeles, Calif., June 29–July 1, 1970; submitted August 3, 1970; revision received November 29, 1970. This work was partially supported by the United States Air Force, Contract F33615-69-C-1336, monitored by the Flight Dynamics Laboratory, Wright-Patterson Air Force Base, Ohio, and was also supported by the McDonnell Douglas Astronautics Company-Western Division, Independent Research and Development Programs.

* Senior Engineer/Scientist. Member AIAA.
† Staff Engineer. Associate Member AIAA.
‡ Engineer/Scientist.
§ Supervisor. Associate Fellow AIAA.

Introduction

THIS paper describes an attempt to utilize the full capabilities of a Univac 1108 computer to assemble state-of-the-art design methods for analyzing the aerothermodynamic behavior of a slender re-entry vehicle. The computations are based on a predescribed trajectory; i.e., time histories of altitude, attitude, and velocity. Thus, coupling between the aerothermodynamic analysis and the trajectory calculation is neglected. However, the analysis includes coupling between the ablating heat shield thermochemistry and the external flowfield calculations. The goal was to produce a program capable of simulating an entire flight in 15 to 30 min on the computer. As a result, the design methods that have evolved are necessarily based upon a series of rational approximations which hopefully attain reasonable accuracy

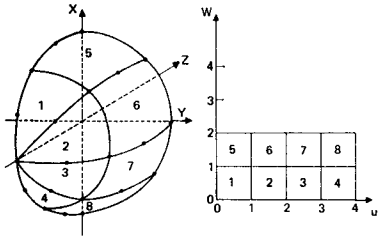

Fig. 1 Patch definition for a typical nosecap.

with minimum complexity. An attempt will be made to describe most of methods[1] used.

Geometrical Considerations

A critical examination of available methods for defining the vehicle geometry led to the selection of a parametric interpolation scheme that maps the entire vehicle surface into a rectangular region in the parametric plane and provides an accurate means of interpolating point locations, surface normals, and surface curvatures. Points are distributed along curves generally oriented in the axial direction. Each curve is fit with a parametric cubic spline and subdivided into a series of equal-length segments. By connecting these nodal points from one curve to the next, the surface is covered by a network of uniformly distributed regions referred to as patches (Fig. 1). The arc lengths of the patch boundaries are appropriately nondimensionalized such that each patch is mapped into a unit square. The actual interpolation equation may be written in matrix form as

$$\mathbf{r} = UM\mathbf{B}M^TW^T \tag{1}$$

where U and W are the arrays $(u^3,u^2,u,1)$ and $(w^3,w^2,w,1)$, respectively, M is the matrix

$$M = \begin{bmatrix} 2 & -2 & 1 & 1 \\ -3 & 3 & -2 & -1 \\ 0 & 0 & 1 & 0 \\ 1 & 0 & 0 & 0 \end{bmatrix} \tag{2}$$

and $\mathbf{B}$ is the matrix of patch corner-point conditions:

$$\mathbf{B} = \begin{bmatrix} \mathbf{r}(0,0) & \mathbf{r}(0,1) & \frac{\partial \mathbf{r}}{\partial w}(0,0) & \frac{\partial \mathbf{r}}{\partial w}(0,1) \\ \mathbf{r}(1,0) & \mathbf{r}(1,1) & \frac{\partial \mathbf{r}}{\partial w}(1,0) & \frac{\partial \mathbf{r}}{\partial w}(1,1) \\ \frac{\partial \mathbf{r}}{\partial u}(0,0) & \frac{\partial \mathbf{r}}{\partial u}(0,1) & \frac{\partial^2 \mathbf{r}}{\partial u \partial w}(0,0) & \frac{\partial^2 \mathbf{r}}{\partial u \partial w}(0,1) \\ \frac{\partial \mathbf{r}}{\partial u}(1,0) & \frac{\partial \mathbf{r}}{\partial u}(1,1) & \frac{\partial^2 \mathbf{r}}{\partial u \partial w}(1,0) & \frac{\partial^2 \mathbf{r}}{\partial u \partial w}(1,1) \end{bmatrix} \tag{3}$$

The derivatives $\partial \mathbf{r}/\partial w$ are determined from the original spline fits of the meridian curves, whereas $\partial \mathbf{r}/\partial u$ and $\partial^2 \mathbf{r}/\partial u \partial w$ are determined from spline fits of $\mathbf{r}$ and $\partial \mathbf{r}/\partial w$ in the u direction.

One of the major numerical computations performed by the computer program is the integration of local pressure and shear loads to obtain vehicle force and moment coefficients,

$$C_x = (1/A_{\text{ref}}) \int_S \int (C_{f\infty} \hat{i} - C_p \hat{n}) dS \tag{4}$$

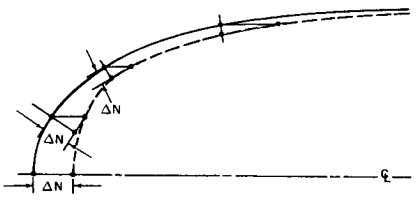

Fig. 2 Geometrical recession procedure.

$$C_{m_x} = (1/A_{\text{ref}} L_{\text{ref}}) \int_S \int \mathbf{r}_{CG} \times (C_{f\infty} \hat{i} - C_p \hat{n}) dS \tag{5}$$

The integrals are evaluated using a Gaussian integration scheme,

$$\int_S \int F(x,y,z) dS = \sum_{i=1}^{Np} \int_0^1 \int_0^1 F(u,w) \left| \frac{\partial \mathbf{r}}{\partial u} \times \frac{\partial \mathbf{r}}{\partial w} \right| du dw \tag{6}$$

$$= \frac{1}{4} \sum_{i=1}^{N_p} \sum_{j=1}^{N_u} \sum_{k=1}^{N_w} W_j W_k F\left(\frac{a_j + 1}{2}, \frac{a_k + 1}{2} \right)$$

where a_j and W_j are the zeros and weighting functions associated with Legendre polynomials of order N_u, and N_p is the total number of patches.

Finally, one of the most perplexing problems encountered during the present study was related to the geometrical aspects of vehicle shape change due to ablation. The transient shape change problem has two types of instability associated with it. The first is purely geometrical, whereas the second is caused by local boundary-layer transition on the nose cap. The geometric instability is well-known to investigators of the two-dimensional/axisymmetric shape change problem. The usual approach to the problem is to follow the behavior of a large number of discrete points and estimate slopes through various linear or quadratic approximations. A very small time step is required. The three-dimensional problem is much more complicated since the surface normal has an additional degree of freedom. Furthermore, the stable time step appears to be inversely proportional to the number of points considered. The present parametric interpolation scheme is good in this respect, since it requires a minimum number of points to accurately describe an arbitrary surface. The stable time step is also dependent on the mechanism used to recess a point. The usual approach is to recess a point along the surface normal. This leads to a bunching of points along the vehicle centerline and a small stable time step. It was found that by projecting the recessed point parallel to the vehicle axis, the geometric instability could be virtually eliminated (see Fig. 2). The following expressions were used to recess the points:

$$\left.\begin{aligned} X_{i+1} &= X_i \qquad Y_{i+1} = Y_i \\ Z_{i+1} &= Z_i - \Delta N / n_z \end{aligned}\right\} \text{ if } |n_z| > \epsilon \tag{7a}$$

$$\left.\begin{aligned} X_{i+1} &= X_i - \Delta N n_x (1 - n_z^2/\epsilon^2) \\ Y_{i+1} &= Y_i - \Delta N n_y (1 - n_z^2/\epsilon^2) \\ Z_{i+1} &= Z_i - \Delta N n_z [1 + (1 - n_z^2)/\epsilon^2] \end{aligned}\right\} \text{ if } |n_z| < \epsilon \tag{7b}$$

The problems associated with local transition on the nose cap are more complex, since the difficulty is not purely geometrical but involves heat transfer prediction in the transition zone. The characteristic transition spike occurs when transition on the nose cap yields a discontinuous rise in the local heating rates. This situation causes much higher recession rates in the turbulent region, and since the laminar region recesses much more slowly, it soon forms a slender protuberance. When a large number of discrete points are examined and transition is assumed to occur abruptly, this behavior is self-preserving, and the protuberance will continue to grow. In the present analysis, the problem is alleviated to some extent by the use of fewer points and by interpolating heat transfer between control points. The latter procedure is identical to assuming a finite-length transition zone.

Local Flow Properties

The rapid design estimation of local flow properties has been improved considerably in recent years. For the most part, the pressure is still obtained using a local-inclination

approach, and the skin-friction determination is still based on the assumption of local similarity. The difference is the sophistication of the empiricism which is now possible with fast computers.

The local pressure is determined through a tangent-cone application of a blunt-cone pressure correlation. The available correlations were unacceptable for the present study, either because of an insufficient range of parameters or because of inherent discontinuities. A blunt-body/method-of-characteristics computer program was exercised for a wide range of cone angles, Mach numbers, and bluntness ratios. The resulting pressures were surface fit using a simplified four-dimensional extension of the parametric interpolation scheme discussed previously, providing continuous values of pressure ratio for $M_\infty \geq 4$, $\theta_c \geq 0$ and $Z/r_N \geq 0$. Given the pressure and the entropy level, T,ρ, and M may be determined by using a surface fit Mollier diagram established for equilibrium air.

Values of local skin friction and heat transfer rates are also required. These quantities require the specification of the viscosity coefficient represented empirically as a function of p and T by Hansen.[2] The problem of estimating the heat transfer at a given point on the vehicle is further complicated by the shape change requirement that the distribution be continuous. The following empirical approach was used: In the neighborhood of the stagnation point the heat transfer can be estimated using the stagnation point solution of Hoshizaki[3] in conjunction with the laminar distribution developed by Lees.[4] Away from the stagnation point where the pressure gradient is relatively small, Eckert's reference enthalpy method can be used for both laminar and turbulent flow. A weighting function was sought which would smoothly switch to the reference enthalpy method away from the nose cap. One such expression which seemed to yield reasonable results was

$$N_c = N_{c_{sp}}(1 - \eta) + N_{c\mathrm{RE}}\eta \tag{8}$$

where

$$\eta = [\tanh(2s/\pi r_N)]^{1/2} \tag{9}$$

This approach also serves to reduce the over-prediction of the reference enthalpy method in regions of large pressure gradient.

In order to obtain values of running length required in the aforementioned calculations as well as the line of action for the shear force, a means of approximating the surface streamline pattern is required. The Newtonian flow model provides that a stream of particles impinging on a surface retains its tangential component of momentum. Thus, at each point on the body, an instantaneous velocity direction is defined by

$$\hat{t} = [\hat{n} \times (\mathbf{u}_\infty \times \hat{n})]/|\hat{n} \times (\mathbf{u}_\infty \times \hat{n})| \tag{10}$$

By writing

$$-\hat{t} = \mathbf{dr}/ds = (\partial \mathbf{r}/\partial u)(du/ds) + (\partial \mathbf{r}/\partial w)dw/ds \tag{11}$$

the derivatives, du/ds and dw/ds, may be solved for and the streamline continued upstream from an arbitrary point on the body until the stagnation point is reached.

To make quantitative estimates of various effects on the local flow properties, the total displacement and momentum boundary-layer thicknesses must be calculated. For a laminar boundary layer, the solutions of Cohen and Reshotko[5] are used with the additional assumption of a zero pressure gradient. This additional assumption is consistent with the use of the reference enthalpy method to predict skin friction and heat transfer. The resulting thicknesses are

$$\frac{\delta_0}{s} = \left(\frac{C_e}{R_{e_s}}\frac{2}{2\sigma + 1}\right)^{1/2}\left(0.4696\,\frac{T_T}{T_e} + 1.217\,\frac{T_w}{T_e} + 1.80\right) \tag{12a}$$

$$\frac{\delta_0^*}{s} = \left(\frac{C_e}{R_{e_s}}\frac{2}{2\sigma + 1}\right)^{1/2}\left[0.4696\left(\frac{T_T}{T_e} - 1\right) + 1.217\,\frac{T_W}{T_e}\right] \tag{12b}$$

$$\delta_0^{**}/s = 0.4696[(C_e/R_{e_s})(2/2\sigma + 1)]^{1/2} \tag{12c}$$

where the Chapman-Rubesin constant C_e is given by

$$C_e = \mu_w T_e/\mu_e T_w = \mu_w \rho_w/\mu_e \rho_e \tag{13}$$

When the boundary layer is turbulent, a velocity profile of the form $\bar{u} = u/u_e = (y/\delta_0)^{1/j}$ is assumed. Using Crocco's integral to express ρ/ρ_e as a function of $\bar{u}$, the thicknesses may be written as

$$\delta_0 = sC_{f_0}/[2j(\sigma + 0.8)(I_{j+1} - I_j)] \tag{14a}$$

$$\delta_0^* = sC_{f_0}(1 - jI_j)/[2j(\sigma + 0.8)(I_{j+1} - I_j)] \tag{14b}$$

$$\delta_0^{**} = \tfrac{1}{2}sC_{f_0}/(\sigma + 0.8) \tag{14c}$$

where

$$I_j = \int_0^1 \frac{h_e \bar{u}^j d\bar{u}}{h_w + (h_T - h_w)\bar{u} + (h_e - h_T)\bar{u}^2} \tag{15}$$

The integral may be evaluated in closed form, but it was found that the resulting expression was poorly behaved, in a numerical sense, for certain combinations of the enthalpies. Consequently, the integral is evaluated numerically using Gaussian quadrature to obtain more reliable results. While any value of j is permissible, most sources advocate the use of $j = 7$.

Mass Addition

Transpiration or heat shield ablation increases the boundary-layer thickness and reduces the skin friction. A typical empirical correlation provides the skin-friction reduction factor as a function of blowing rate, boundary layer edge conditions, and properties of the injected species. Defining the blowing parameter,

$$B = \dot{m}_w/(\rho u)_e C_{H_0} \tag{16}$$

the skin-friction reduction can be represented using the following empirical expressions:

$$C_f/C_{f_0} = C_H/C_{H_0} = 1.0 - 0.68G^{0.4}B + 0.08G^{0.4}B^2 \quad \text{(Laminar)} \tag{17a}$$

$$C_f/C_{f_0} = C_H/C_{H_0} = G^{0.8}B/(1 + G^{0.8}B/4)^4 - 1 \quad \text{(Turbulent)} \tag{17b}$$

where G is the ratio of the mean specific heat of the injected species to that of air at wall conditions.

The momentum and displacement thicknesses are modified[6] as

$$\delta^{**}/\delta_0^{**} = \delta^*/\delta_0^* = C_f/C_{f_0} + B \tag{18}$$

whereas the total thickness is written[6,7] as

$$\delta/\delta_0 = F_L\delta^{**}/\delta_0^{**} \quad \text{(Laminar)} \tag{19a}$$

$$\delta/\delta_0 = F_T\delta^{**}/\delta_0^{**} \quad \text{(Turbulent)} \tag{19b}$$

The function F_L varies monotonically from 0.6 to 1.0 as M_e increases from zero. Since M_e will ordinarily be quite large in most of the afterbody applications, it is reasonable to assume $F_L = 1$. The turbulent function F_T is only a weak function of M_e and may be approximated by

$$F_T = (1 + 0.143B)^{-1} \tag{20}$$

Transverse Curvature

In cases where δ is large compared with the local body radius, the transverse curvature effect must be in the boundary-layer solutions. Qualitatively, the effect of transverse curvature is to decrease δ and correspondingly increase the skin friction and heat transfer. For laminar flow, the results of Probstein and Elliott[8] are used. In a manner similar to that used to include the effect of mass addition, values of skin-friction coefficients and the various boundary-layer thicknesses, divided by their uncorrected values, may be written as simple functions of the transverse curvature parameter, $\zeta \sim \delta \cos\theta_c/r_w < 1$. If the boundary layer is turbulent, the transverse curvature effect is not well established but is small. Consequently, it was decided to neglect the transverse curvature effects for turbulent flow. When the combined effects of transverse curvature and mass addition are considered, the various quantities may be computed in a similar manner to that shown here for C_f:

$$C_f = (C_{f_{tvc}}/C_{f_0})_{B=0} \times (C_f/C_{f_0})_{\zeta=0} \times (C_{f_0})_{\substack{B=0 \\ \zeta=0}} \quad (21)$$

Cross Flow

At small angles of attack, the boundary layer becomes thinner over the windward surfaces and thicker over the leeward surfaces. Small cross flow ($\alpha/\theta_c \leq 1$) may be treated[9,10] by modifying the total and displacement boundary-layer thicknesses according to

$$\delta_0/\bar{\delta}_0 = \delta_0^*/\bar{\delta}_0^* = \exp(-2\alpha/\theta_c \cos\phi) \quad (22)$$

where the barred quantities refer to the zero-angle-of-attack values, whereas ϕ is the meridian angle measured from the windward meridian. When $\alpha/\theta_c > 1$ the cross flow may cause the boundary layer to separate. Based on compiled data,[11] the following correlation is used to predict the separation meridian angle:

$$\phi_s = \max(\phi_{s1}, \phi_{s2}) \quad (23)$$

where

$$\begin{aligned} \phi_{s1} &= 123.5 + 0.256 \tan^{-1}(0.21\theta_c) \\ \phi_{s2} &= 180 + (0.867\theta_c - \alpha)(17 - 1.15\theta_c + 0.0278\theta_c^2) \end{aligned} \quad (24)$$

The pressure is calculated by using a Prandtl-Meyer expansion between the shadow line and the separation line. A sinusoidal distribution is assumed between the separation point and the leeward meridian with the maximum recompression assumed to be given approximately by the following expression:

$$(p_{lee} - p_{min}/p_\infty - p_{min}) = \tfrac{1}{2} \quad (25)$$

Viscous Interaction and Stream Tube Calculation

The key problem here seems to be the selection of the proper means of estimating the effective body profile. Fannelop[12] and Burggraf[13] developed similar expressions for the effective boundary-layer displacement thickness including mass addition,

$$\Delta^* = \delta^* + \frac{1}{\rho_e u_e r_w^\sigma} \int_0^s \dot{m}_w r_w^\sigma ds \quad (26)$$

Considering once again the zero pressure gradient similar solution, Eq. (26) becomes

$$\Delta^* = \delta^* + \dot{m}_w s/[\rho_e u_e(\sigma + i + 1)] \quad (27)$$

where $i = -0.5$ for the laminar case; $i = -0.2$ for the turbulent case. The effective local inclination is given by

$$\xi_{eff} = \xi_0 + (i+1)\delta^*/s + (i+1)m_w/[\rho_e u_e(\sigma + i + 1)] \quad (28)$$

The induced pressure *increment* is evaluated using a conventional tangent-cone pressure law:[14]

$$C_p/\xi^2 = 1 + [(\gamma+1)K^2 + 2]/(\gamma-1)K^2 + 2 \ln\left[\left(\frac{\gamma+1}{2}\right) + K^{-2}\right] \quad (29)$$

Thus, the induced pressure increment is given by

$$\Delta p = p(K,\xi) - p(K_0,\xi_0) \quad (30)$$

When the vehicle under consideration has a blunt nose, there will be a significant entropy variation along the boundary-layer edge. Near the nose, the entropy level of the streamline merging with the boundary layer is governed by a nearly normal shock. As the flow proceeds downstream, continuity requires the stream tube radius to increase until the limiting case of the sharp cone shock angle is reached. Since the present analysis does not include a complete flowfield solution, an empirical shock shape is required.[15] Mass addition is assumed to be small compared with the mass flow in the boundary layer. A simple mass balance yields the radius at which the merging streamline crossed the shock,

$$r = [2r_w(\delta_0 - \delta_0^*)\rho_e u_e/\rho_\infty u_\infty]^{1/2} \quad (31)$$

which is sufficient to define the shock angle β_s using the empirical shock shape. However, since the boundary-layer thicknesses and edge conditions are strongly dependent on the edge entropy, the viscous interaction and approximate stream tube calculations are interdependent and require an iterative solution. Numerically, the problem is to solve a pair of highly complicated implicit relationships for two unknowns (in this case, β_s and $d\delta^*/ds$). A Newton-Raphson approach provides rapid convergence.

Boundary-Layer Transition

It has been observed the local boundary-layer transition can have a significant effect on the aerodynamic characteristics of a slender re-entry vehicle. Unfortunately, the problem of accurately predicting local boundary-layer transition has thus far defied analysis. Hence, an empirical transition criterion must be used.

There are two ways to approach this problem. A general, nonablating transition Reynolds number could be defined empirically and the appropriate reduction due to ablation added as a correction, as in the case of the skin-friction reduction. The approach used for this paper was to predict empirically the actual ablating transition Reynolds number directly based on flight test results for a particular ablative material. Specifically, for a carbon-phenolic heat shield, the following expression was used:

$$\log_{10} R_{et} = 5.37 + 0.2325 M_e - 0.004015 M_e^2 \quad (32)$$

Base Flow

Most methods available for predicting base pressure were developed for two-dimensional flow. The axisymmetric theories, normally restricted to very specific conditions, are difficult to modify for the complicated flowfields being considered in the present study. Thus, the base pressure method must be reasonably accurate for engineering applications, and also sufficiently flexible to enable it to be modified to achieve compatibility with the complex flowfield calculations described previously. The Chapman-Korst base-flow model and modified theories based on that model appear to be particularly amenable to the present problem. These modified theories are capable of handling a) an initial boundary-layer effect such as surface mass addition, b) axisymmetric flow, c) laminar and turbulent flow, d) base injection, e) transient base pressure, and f) supersonic to hypersonic flow.

There is a thorough review of these theories.[16] Recently, a simplified axisymmetric base-flow theory has been developed

which uses the two-dimensional theories by transforming the axisymmetric equations into an equivalent two-dimensional form. This approach has been used successfully to predict base pressures for cylindrical and conical bodies over a sufficiently wide range of flowfield conditions to satisfy the needs of the present study. There are further details and comparisons with experimental data.[1]

Ablation Analyses

The thermochemical ablation analysis is developed from solutions of the governing conservation equations by Lees[17] that assume unity Lewis, Prandtl, and Schmidt numbers for laminar and turbulent flow. More sophisticated solutions to the multicomponent chemically reacting system, e.g., Gilbert and Scala[18] and Kendall, et al.,[19] are not warranted and do not appear feasible for a requirement of rapid numerical computation. The internal heat and mass transfer for the charring ablators is represented with a transient differential equation similar to that reported by Moyer and Rindal.[20] For less severe heating environments on a conical heat shield, the thermochemical methods are adequate. However, high-pressure test facilities have revealed large discrepancies between analytical predictions and the observed mass-loss data. The use of empirical correlations of test data for actual flight environments indicates that drastic nose cap shape change may occur. Various analyses of the thermomechanical ablation have been attempted[21-24] but, for the present paper, a simple linear relation is used which provides the thermomechanical factor as a function of stagnation pressure and local flow inclination.

Surface Heat and Mass Transfer

The several energy transfer mechanisms between the boundary layer gas and the ablating surface are shown in Fig. 3.

$$q_s = q_w - \dot{m}_w h_w + \dot{m}_g h_g + \dot{m}_c h_c - q_{RR} + \dot{m}_M h_c + \alpha_s q_R \quad (33)$$

where the mass balance across the surface is given by

$$\dot{m}_w + \dot{m}_M = \dot{m}_c + \dot{m}_g \quad (34)$$

Mechanical and liquid flow removal from a nosecap are accounted for separately in the ablation analysis by semiempirical correlations, i.e., $\dot{m}_M = f(\dot{m}_w, p_{sp}, \xi)$, as described subsequently.

For relating the surface energy and mass balances it is expedient to define

$$B^* = \dot{m}_w/(\rho u)_e C_H \quad (35)$$

Equation (33) is coupled to the boundary-layer solution by assuming unity Lewis, Prandtl, and Schmidt numbers for laminar flow.[17] As a result the energy and species equations are similar and the total enthalpy and the mass fractions of the individual chemical elements satisfy the relationship

$$K_i = K_{iw} + (K_{ie} - K_{iw})(H - h_w)/H_T - h_w \quad (36)$$

where K_{ie} depends upon the boundary conditions. Generally, H_T and K_{ie} are constant along a body, but it is also required that h_w and K_{iw} be either constant or slowly varying along the surface. Equation (36) is independent of the momentum equation. By substituting it into the conservation of species equation for known boundary conditions the following relationships are obtained: for freestream elements;

$$K_{iw} = K_{ie}/(B^* + 1) \quad (37)$$

and for the ablation or transpiration elements;

$$K_{jw} = \dot{m}_{jw}/(\rho u)_e C_H (B^* + 1) \quad (38)$$

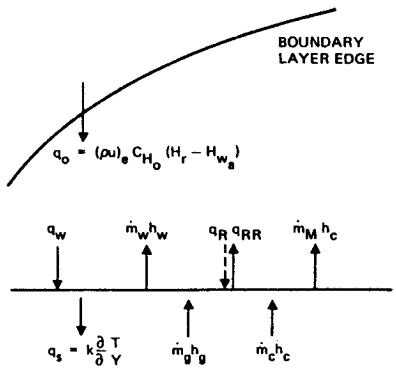

Fig. 3 Surface energy balance mechanisms.

For turbulent flow the turbulent value of C_H replaces the laminar value, as shown by Lees.[17] The effects of mass transfer are included in the Stanton number C_H.

Equation (35) can be substituted into Eq. (33) and the result can be shown to be similar to energy balance relationships.[17] This step is not shown and the energy balance is presented in a form which is physically more meaningful; the heat flux to the surface is seen to be given by a convection term and a combustion term:

$$q_s = (\rho u)_e C_H (H_r - h_{w_a}) - \dot{m}_w \Delta Q + \dot{m}_g h_g + \dot{m}_c h_c - q_{RR} + \alpha_s q_R \quad (39)$$

where

$$\Delta Q = \frac{\dot{m}_g}{\dot{m}_w}(h_g + \Delta h_g^0) - \frac{\dot{m}_c}{\dot{m}_w}(h_c + \Delta h_c^0) - \left(\frac{1}{\sum_{j=1}^{n} K_{jw}} - 1\right) h_{w_a} + \frac{1}{\sum_{j=1}^{n} K_{jw}} h_w \quad (40)$$

The enthalpy of the products h_w is obtained from a thermochemical equilibrium program. The convective heating contribution is determined by an environment enthalpy potential and thus is unperturbed by the presence of foreign species at the wall.

The mass transfer value of the Stanton number C_H is related to the nonmass-transfer value of C_{H_0} by the empirical correlations given in Eq. (17).

The thermochemistry computations for the enthalpy h_w and specific heat c_{p_w} of the products are performed independently by a separate computer program. For a given ablative material, this program generates the surface equilibrium thermochemistry, including phase changes, as functions of three parameters: 1) pressure, 2) gaseous char mass flux, $\dot{m}_c/(\rho u)_e C_H$, and 3) internal pyrolysis gas or transpirant mass flux, $\dot{m}_g/(\rho u)_e C_H$. Thermochemistry data for graphite ($\dot{m}_g/(\rho u)_e C_H = 0$) are identical to those reported by Kratsch.[23]

The energy balance of Eq. (39) is coupled to the internal heat and mass transfer as described in the following paragraphs.

Internal Heat and Mass Transfer

The limitation of the numerical heat conduction solution usually determine the computation efficiency of a transient charring ablator program. For aerodynamic computations, less accuracy is required for the internal solution than for the ablating surface solution. Some approximations are used with the internal heat and mass transfer solution to reduce computation time; however, the methods combine accuracy with excellent computation efficiency.

The sensible energy exchange is equal to the sum of terms due to conduction, gaseous heat transfer, decomposition, and

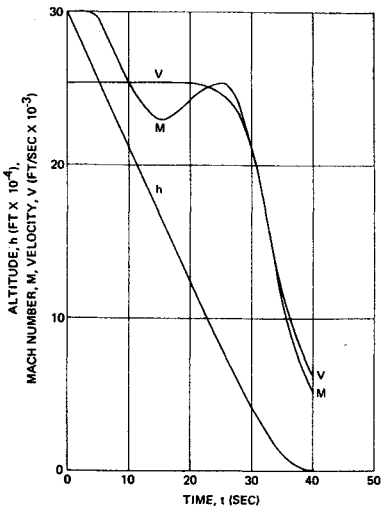

Fig. 4 Trajectory parameters.

the moving coordinate system (recession):

$$\rho c_p \frac{\partial T}{\partial t} = \frac{\partial}{\partial y}\left(k \frac{\partial T}{\partial y}\right) + \dot{m}_g \frac{\partial h_g}{\partial y} + \Delta H_{dp} \frac{\partial \rho_{dp}}{\partial t} + \dot{s}\rho c_p \frac{\partial T}{\partial y} \quad (41)$$

Assumptions constraining the in-depth solution are that a) internal decomposition can be represented by a single Arrhenius rate equation, b) changes in mass flux are sensed instantaneously at the ablating surface, and c) internal radiation is unimportant.

The decomposition gas formation rate is given by

$$\rho_{dp} = \frac{\partial \rho_{dp}}{\partial t} = f_B \rho_0 \left[\frac{\rho - \rho_0(f_B + \gamma' f_B)}{f_B \rho_0 (1 - \gamma')}\right]^n A e^{-E^*/T} \quad (42)$$

The internal gaseous mass transfer is obtained from a mass balance. The pyrolysis heat of decomposition ΔH_{dp_i} is derived from an energy and mass balance and is presented in terms of energy per unit mass of pyrolysis gas formed. The thermal conductivity and specific heat are temperature- and density-dependent.

Numerical shape factors may be used for one-dimensional heat conduction in cylindrical and spherical coordinate systems. The shape factors are particularly useful for nose caps.

A characteristic of charring ablator programs is that the pyrolysis decomposition rates and internal gaseous mass transfer may be overly responsive to the Arrhenius rate equation. An oscillatory response may occur for conditions where surface recession rates are high and temperature profiles are steep. These occurrences have been eliminated for the subprogram by dividing each lamina into 16 sublaminae. The sublaminae density profile is used with the Arrhenius rate equation and the profile is carried through the computation history. A mean lamina density is defined for the heat conduction solution. The density profile is modified to account for surface recession $\dot{s}$ using Newton's backward difference interpolation formula.

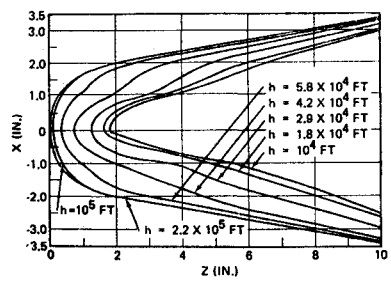

Fig. 5 Nose tip shape change.

The surface and internal heat and mass transfer are coupled at the outer lamina. An energy balance is performed on the lamina by combining Eqs. (39) and (41). The surface temperature T_w is solved for using the Newton-Raphson method.

The transient heat conduction solution is obtained using a fourth-order Runge-Kutta explicit computational procedure. The recovery enthalpy H_r and heat transfer coefficient $(\rho u)_e C_H$ are defined at times of $t_i, t_i + \frac{1}{2}\Delta t$, and $t_i + \Delta t$. An important feature of the numerical solution is that a transformed coordinate system is not used to eliminate the moving boundary condition. Consequently, the lamina thickness is not altered and computing time increments are not decreased as the ablating surface recedes. Laminae are dropped at the back surface.

Thermomechanical Ablation

Empirical correlations of thermomechanical ablation have been developed.[22,23] The ratio of experimental mass flux to thermochemical mass flux was correlated with stagnation enthalpy and pressure. Bishop and DiCristina[22] also relate thermomechanical erosion to surface pressure gradients, aerodynamic shear, and material characteristics such as char thickness and char strength. Semiempirical approaches to thermomechanical erosion predictions have been developed[21,25] in which material performance is related to local fractures and char spallation caused by thermal stresses, internal gasification and surface aerodynamic shear, but these methods are overly complex for the analytical constraints of the current computer code.

We have adapted an empirical approach which is related to the thermochemical ablation rate, stagnation pressure, and local inclination, $\dot{m}_M = f(\dot{m}_w, p_{sp}, \xi)$. Each ablative material requires a different correlation. Further study may also indicate modified correlations for different applications and flight environments. The indicated empirical relation-

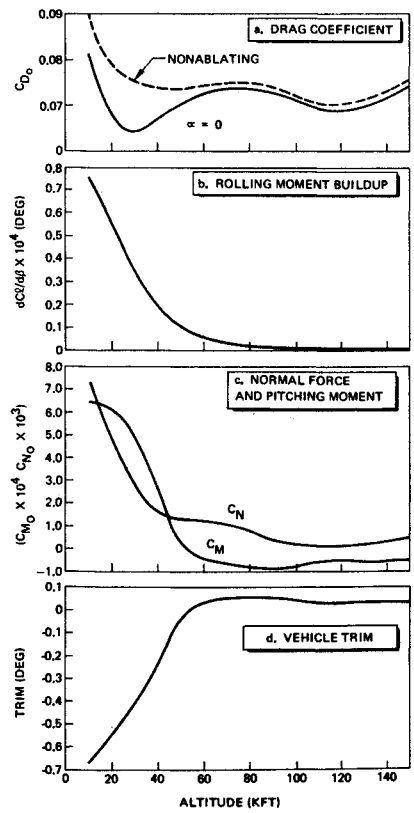

Fig. 6 Effect of asymmetric ablation on total drag coefficient, rolling moment buildup, normal force, and pitching moment, and vehicle trim.

ships are the following:

stagnation point

$$\dot{m}_{M,\mathrm{sp}}/\dot{m}_{w,\mathrm{sp}} = (A_\gamma + B_\gamma P_{\mathrm{sp}})^{-1} \tag{43a}$$

nose cap

$$\dot{m}_M = \dot{m}_w(\dot{m}_{M,\mathrm{sp}}/\dot{m}_{w,\mathrm{sp}})(A\theta + B_\theta \xi) \tag{43b}$$

where $p_{\mathrm{sp}} \leq p_{\mathrm{crit}}$ (the threshold stagnation pressure). The requirement of continuous surface recession over the nose cap is maintained by these relationships. No additional complexity is introduced by extending the correlating parameters to include stagnation enthalpy, aerodynamic shear, etc.

Example

The following example was selected to demonstrate the program's capability. A 6-ft, 10° cone with a 2-in. nose radius was flown through a ballistic trajectory at a constant 5° angle of attack. The trajectory described in Fig. 4 was generated by a point mass trajectory program with an initial entry angle of 20° at 300 kft and 25 kft/sec. A constant ballistic coefficient of 2,500 psf was assumed. Carbon phenolic was selected as the ablative material. Figure 5 depicts the predicted nose tip shape change history. Figure 6a is a plot of the zero-angle-of-attack drag coefficient vs altitude for both the ablating and the nonablating case. The inviscid drag is essentially unchanged with the difference due to a decrease in both the viscous and base drag. Perhaps equally significant is the growth and magnitude of the rolling moment derivative, $dC_l/d\beta$, as shown in Fig. 6b. The zero-angle-of-attack normal force and pitching moment coefficient histories are presented in Fig. 6c, and Fig. 6d describes the variation of the trim angle of attack due to ablation effects.

Concluding Remarks

This paper has described the essential features of a computer program designed to couple the calculation of the vehicle static aerodynamic characteristics with an accurate thermochemical analysis of the ablating heat shield. A computing time constraint was used in the selection of the individual analyses, but it is felt that even if no such limitation were imposed, the state of the art could not provide any significant improvement in the accuracy. In addition to predicting the aerodynamic performance of ablating re-entry vehicles, this tool was created to serve as a test bed for new methods. With this in mind, the program was coded on a modular basis, so that the individual techniques can be replaced with a minimum effort. It is anticipated that refinements will occur, but that they will not greatly alter the over-all results. Certain aspects of the shape change problem and the heat transfer prediction may be improved. Specific problem areas are a) arbitrary nose shape, b) a uniform approach, valid over the entire vehicle and producing continuous results for laminar and turbulent boundary layers, and c) a better definition of the transition zone. A closely related item also being considered for improvement is the prediction of local boundary-layer transition. Finally, an attempt should be made to reduce the uncertainty associated with the prediction of thermomechanical effects on surface recession.

In attempting to assess the significance of the results obtained in the example, one should keep in mind the fact that this tool represents an intermediate state of development. The ultimate simulation program would include a coupling with the vehicle dynamics. Thus, it is difficult to judge the results generated by a somewhat artificial example with uncoupled dynamics. It is felt that the magnitudes of the asymmetric effects could be important if they were encountered during an actual flight. The next step is to investigate the combination of the present code with a trajectory analysis. The inclusion of ablation effects eliminates the tabular procedure for adding aerodynamics to a trajectory program, since the coefficients may no longer be treated in a quasi-steady manner. The forces and moments acting on the vehicle at a given time now depend on its previous motion. A direct coupling of trajectory and aerothermodynamic analyses would be economically impractical—the computing time would be enormous. The approach which is currently under consideration involves a back-to-back cycling of the two programs, with the aerodynamics program generating linearized characteristics for use in the trajectory program. Hopefully, only a few cycles would be required to achieve a converged trajectory. In a parallel effort, an attempt will be made to include the calculation of the dynamic stability characteristics.

References

[1] Timmer, H. G. et al., "Ablation Aerodynamics for Slender Reentry Bodies, Vol. I—Theoretical Analyses and Results," Rept. MDC-G1285, March 1970, McDonnell Douglas Astronautics Company, Huntington Beach, Calif.

[2] Hansen, C. F. and Heims, S. P., "A Review of the Thermodynamic, Transport, and Chemical Reaction Rate Properties of High Temperature Air," TN4359, July 1958, NACA.

[3] Hoshizaki, H., "Heat Transfer in Planetary Atmospheres at Super-Satellite Speeds," *ARS Journal*, Oct. 1962, pp. 1544–1552.

[4] Lees, L., "Laminar Heat Transfer Over Blunt-Nosed Bodies at Hypersonic Flight Speeds," *Jet Propulsion*, Vol. 26, No. 4, April 1956, pp. 259–269.

[5] Cohen, C. B. and Reshotko, E., "Similar Solutions for the Compressible Laminar Boundary Layer With Heat Transfer and Pressure Gradient," Rept. 1293, 1956, NACA.

[6] Walker, G. K. and Schumann, B. A., "The Growth of Turbulent Boundary Layers," MSVD TIS R61SD123, July 1961, General Electric, King of Prussia, Pa.

[7] Walker, G. K., "The Growth of Laminar Boundary Layers with Zero Pressure Gradient," TFM 8151-008, Jan. 1963, General Electric, King of Prussia, Pa.

[8] Probstein, R. F. and Elliott, D., "The Transverse Curvature Effect in Compressible Axially Symmetric Laminar Boundary Layer Flow," *Journal of the Aeronautical Sciences*, Vol. 28, No. 3, March 1956, pp. 208–223.

[9] Tracy, R. R., "Hypersonic Flow Over a Yawed Circular Cone," Memo. 69, Aug. 1963, Firestone Flight Sciences Lab., California Inst. of Technology, Pasadena, Calif.

[10] Cross, E. J. Jr. and Hankey, W. L., "Investigations of the Leeward Side of Delta Wing at Hypersonic Speeds," AIAA Paper 68-675, Los Angeles, Calif., 1968.

[11] Chang, P. K. et al., "Analysis of Laminar Flow and Heat Transfer on a Hypersonic Cone at High Angle of Attack," TR 2, Aug. 1968, The Catholic University of America, Washington, D.C.

[12] Fannelop, T. K., "Displacement Thickness for Boundary Layers With Surface Mass Transfer," *AIAA Journal*, Vol. 4, No. 6, June 1966, pp. 1142–1144.

[13] Burggraf, O. R., "Choice of Boundary Conditions in Viscous Interaction Theory," *AIAA Journal*, Vol. 4, No. 6, June 1966, pp. 1145–1146.

[14] Rasmussen, M. L., "On Hypersonic Flow Past an Unyawed Cone," *AIAA Journal*, Vol. 5, No. 8, Aug. 1967, pp. 1495–1497.

[15] Billig, F. S., "Shock Wave Shapes Around Spherical- and Cylindrical-Nosed Bodies," *Journal of Spacecraft and Rockets*, Vol. 4, No. 6, June 1967, pp. 822–823.

[16] Tang, H. H., Gardiner, C. P., and Barnes, J. W., "Jet Mixing Theories, Extensions and Applications in Separated Flow Problems," DAC-59181, Feb. 1967, Douglas Aircraft Co., Santa Monica, Calif.

[17] Lees, L., "Convective Heat Transfer With Mass Addition and Chemical Reactions," *Combustion and Propulsion, Third AGARD Colloquium*, Pergamon Press, New York, 1958.

[18] Gilbert, L. M. and Scala, S. M., "Combustion and Sublimation of Cones, Spheres, and Wedges at Hypersonic Speeds," *AIAA Journal*, Vol. 3, No. 11, Nov. 1965, pp. 2124–2131.

[19] Kendall, R. M. et al., "An Analysis of the Coupled Chemically Reacting Boundary Layer and Charring Ablator," CR-1060, June 1968, NASA.

[20] Moyer, C. B. and Rindal, R. A., "Finite Difference Solution for the In-Depth Response of Charring Materials Considering Surface Chemical and Energy Balances," Final Rept. 66-7, Pt. II, March 1967, Vidya Div., Itek Corp., Palo Alto, Calif.

[21] Mathieu, R. D., "Mechanical Spallation of Charring Ablators in Hyperthermal Environments," *AIAA Journal*, Vol. 2, No. 9, Sept. 1964, pp. 1621–1627.

[22] Bishop, W. M. and DiCristina, V., "A Prediction Technique for Ablative Material Performance Under High Shear Re-Entry Conditions," *AIAA Journal*, Vol. 6, No. 1, Jan. 1968, pp. 59–63.

[23] Kratsch, K. M. et al., "Graphite Ablation in High-Pressure Environments," AIAA Paper 68-1153, Williamsburg, Va., 1968.

[24] McVey, D. F., Auerbach, I., and McBride, D. D., "Some Observations on the Influence of Graphite Microstructure on Ablation Performance," AIAA Paper 70-155, New York, 1970.

[25] Schneider, P. J., Dolton, T. A., and Reed, G. W., "Mechanical Erosion of Charring Ablators in Ground-Test Reentry Environments," *AIAA Journal*, Vol. 6, No. 1, Jan. 1968, pp. 64–72.

APRIL 1971 J. SPACECRAFT VOL. 8, NO. 4

Measurements of the Dynamical Behavior of Projectiles over Long Flight Paths

WILLIAM H. MERMAGEN*
Ballistic Research Laboratories, Aberdeen Proving Ground, Md.

The yawing and rolling behavior of projectiles is studied using a pair of onboard solar aspect sensors. The instrumentation and data handling procedures used to extract motion information from the data are discussed. Several interesting flights of fin- and spin-stabilized shells are described in detail. Large-amplitude yawing motion and roll reversal with the possibility of resonance have been observed. The pitch frequencies are well determined, and the derived modal amplitudes and phases seem reasonable. Applications and limitations of the technique are discussed.

Nomenclature

C_{M_α} = static moment coefficient
c_0, c_2 = cubic static moment coefficients
I_x, I_y = axial, transverse moments of inertia
K_j = amplitude of the j − mode (j = 1,2)
K_s = amplitude of the projection of the unit solar vector onto the Y-Z plane of the fixed plane coordinate system
k_t = transverse radius of gyration
l = reference length (body diameter)
M_2 = a combination of the linear and nonlinear parts of the cubic static moment
m_j = direction cosines of the unit missile vector (j = 1,2,3)
P = gyroscopic spin
S = reference area ($\pi l^2/4$)
s_j = direction cosines of the unit solar vector (j = 1,2,3)
s = distance along the trajectory (arc length)
t = time
$\mathbf{u}_s$ = unit vector in the direction of the sun
$\mathbf{u}_m$ = unit vector along the missile axis
V = velocity
x = interval between successive sun-sensor pulses
y = interval between alternate sun-sensor pulses
α_t = total angle of attack
β = half-angle between solar sensors on the circumference of the missile
γ = cos α_t
γ_j = angle of inclination between the field of view of the jth sensor and the missile axis (j = 1,2)
ϕ = roll angle
ϕ_j = phase angle of the j modal arm (j = 1,2)
ϕ_s = phase angle of the solar modal arm
λ_j = damping rate of the j modal amplitude (j = 1,2)
ρ = density of air
σ = solar aspect angle (between missile axis and solar vector)
ξ, ξ_g = complex yaw, and complex yaw of repose
ξ_s = complex solar orientation

Superscripts

$(\dot{}), (\ )'$ = $d(\ )/dt$ and $d(\ )/ds$, respectively

Subscripts

0 = initial conditions or zero order
r = reduction or average value

Presented as Paper 70-538 at the AIAA Atmospheric Flight Mechanics Conference, Tullhama, Tenn., May 13–15, 1970; submitted May 28, 1970; revision received December 10, 1970.

* Chief, Physical Measurement Section, Exterior Ballistics Laboratory. Member AIAA.

Introduction

THE pitching, yawing, and rolling motion of projectiles is usually measured in wind tunnels and free-flight ranges using shadowgraph techniques. Until recently no direct measurements of projectile motion over long trajectories have been possible because of the limitations of ground-based instruments. Advances in the art of high-g telemetry have permitted the instrumentation of projectiles with active electronic payloads.[1–5] These onboard instruments are designed to survive accelerations up to 100,000 g during gun-launch. Solar aspect sensors[6] and accelerometers have been developed to observe the motion of the projectile. A yawsonde built by the British and used by the Naval Weapons Center (NWC) China Lake, in a small number of flights.[7] A Harry Diamond Laboratories modification of this sonde has also been used by NWC.

The Ballistic Research Laboratories have developed a yawsonde of different design and have successfully instrumented a number of projectiles to obtain data on yawing and rolling motion. This paper describes the onboard solar aspect sensing instrument, calibration and analysis techniques, data handling and reduction processes (manual and automated), accuracy limitations, results of recent firings, and limitations of and usefulness of this technique.